This is an open access article published under a Creative Commons Attribution (CC-BY) License, which permits unrestricted use, distribution and reproduction in any medium, provided the author and source are cited.

CHEMISTRY OF MATERIALS

Review

pubs.acs.org/cm

Engineering Valence Band Dispersion for High Mobility p-Type Semiconductors

Benjamin A. D. Williamson,[†] John Buckeridge,[†] Jennilee Brown,[†,¶] Simon Ansbro,[†,¶] Robert G. Palgrave,[†,¶] and David O. Scanlon*[,†,‡]

[†]University College London, Kathleen Lonsdale Materials Chemistry, Department of Chemistry, 20 Gordon Street, London WC1H 0AJ, United Kingdom

[‡]Diamond Light Source Ltd., Diamond House, Harwell Science and Innovation Campus, Didcot, Oxfordshire OX11 0DE, United Kingdom

[¶]University College London, Department of Chemistry, Christopher Ingold Building, London WC1H 0AJ, United Kingdom

ABSTRACT: The paucity of high performance transparent p-type semiconductors has been a stumbling block for the electronics industry for decades, effectively hindering the route to efficient transparent devices based on p−n junctions. Cu-based oxides and subsequently Cu-based oxychalcogenides have been heavily studied as affordable, earth-abundant p-type transparent semiconductors, where the mixing of the Cu 3d states with the chalcogenide 2p states at the top of the valence band encourages increased valence band dispersion. In this article, we extend this mixing concept further, by utilizing quantum chemistry techniques to investigate ternary copper phosphides as potential high mobility p-type materials. We use hybrid density functional theory to examine a family of phosphides, namely, MCuP (M = Mg, Ca, Sr, Ba) which all possess extremely disperse valence band maxima, comparable to the dispersion of excellent industry standard n-type transparent conducting oxides. As a proof of concept, we synthesized and characterized powders of CaCuP, showing that they display high levels of p-type conductivity, without any external acceptor dopant. Lastly, we discuss the role of Cu-coordination in promoting valence band dispersion and provide design principles for producing degenerate p-type materials.

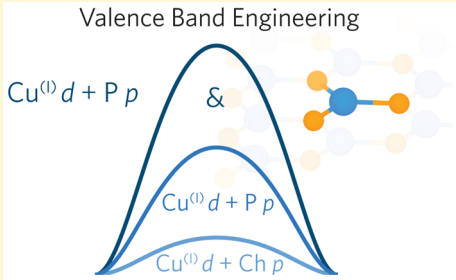

■ INTRODUCTION

Devices based on p−n junctions have revolutionized our lives, being ubiquitous in modern consumer electronics such as smartphones, tablets, laptops, and flat screen displays as well as pushing the boundaries of renewable energy.[1−5] Transparent p−n junctions represent a major area where the lack of a wide band gap *degenerate* p-type material has limited the progress of such devices, despite the huge successes seen with their n-type transparent conducting oxide (TCO) counterparts. The field of solar cells can also benefit from a highly conducting transparent p-type material as they provide good ohmic contact and band matching to the solar absorber, unlike their n-type counterparts.[6−8] Over half a century of research has failed to produce a high performance p-type TCO, meaning they are used as passive electrodes and as such limit the fulfilment of *"transparent electronics"*.[4]

Initial attempts at designing p-type TCOs focused on acceptor doping of the high performance n-type TCOs (e.g., In_2O_3, ZnO, SnO_2)[9−14] and is in fact still currently attempted.[15,16] The thinking behind this procedure is that the fabrication of a p−n homojunction would be relatively facile if p-type SnO_2 was to be combined with n-type SnO_2, for example. Recent theoretical studies have pointed out that due to the large electron affinities and ionization potentials of these systems[17−20] there is a thermodynamic driving force for n-type defects (excess electrons) increasing the probability that even if holes could form they would result in immediate compensation by intrinsic donor defects under all growth conditions.[10,11,13] In addition to this, the localized O 2p states at the top of the valence band promote a tendency to form polaronic defects localized on oxygen sites.[11] These factors all indicate that it is extremely unlikely that these n-type TCOs can ever be turned into p-type.

Initial attempts at designing p-type TCOs came in the form of the *"Chemical Modulation of the Valence Band"* (denoted CMVB herein) as proposed by Hosono and co-workers in 1997.[21] The authors reported that $CuAlO_2$, which crystallizes in the delafossite structure possessed both native p-type conductivity and optical transparency.[21] It was noted that the Cu 3d−O 2p mixing in the valence band of Cu_2O mediated a smaller ionization potential than most binary oxides, promoted an increased valence band dispersion, and favored p-type conductivity.[22−24]

Hosono postulated that a ternary Cu-based oxide could provide a larger fundamental band gap while retaining the valence band features of Cu_2O. Other delafossite TCOs such as

Special Issue: Computational Design of Functional Materials

Received: August 10, 2016
Revised: October 14, 2016

 © XXXX American Chemical Society

DOI: 10.1021/acs.chemmater.6b03306
Chem. Mater. XXXX, XXX, XXX−XXX

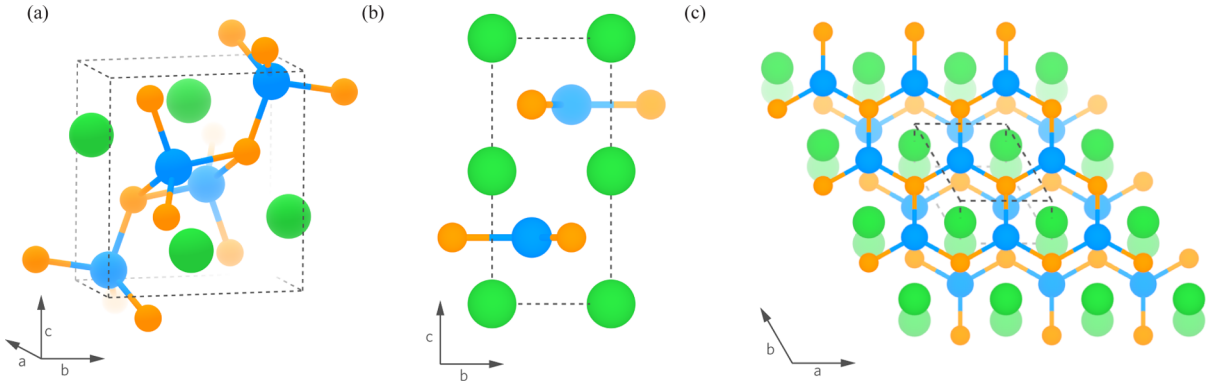

Figure 1. Crystal structure of (a) MgCuP (*Pnma*) displaying the tetrahedrally coordinated Cu. The crystal structure of MCuP ($P6_3/mmc$) is shown in (b) as viewed along the (100) direction and (c) shown down the *c*-axis displaying the hexagonal layered network of trigonally planar coordinated Cu−P and the M(II) cations in the void between the layers. M(II) is colored green, Cu is blue, and P is shown in orange. Bonds have been made between Cu and P, and the unitcell is represented with a dashed line.

$CuMO_2$ (M = B,[25,26] Sc,[27,28] Cr,[29] Ga,[28,30] Y,[28] In,[28] La[28]) and also $SrCu_2O_2$[31,32] were identified where, in each case, Cu is linearly coordinated to two oxygens in a O−Cu−O dumbbell-like motif.[21,33] It was also postulated that it was important to break the localization of electrons on the oxygen 2p states through a tetrahedral coordination reducing the nonbonding nature of the ions as all the electrons are distributed along the four σ bonds and thus no lone pairs are formed.[34]

Although these Cu-based oxides were transparent and displayed p-type conductivity, their conductivities were typically orders of magnitude smaller than that of their n-type counterparts. It has subsequently been demonstrated that the ionization levels of acceptor defects in these systems are quite deep in nature,[35−39] meaning that degenerate conductivity is virtually impossible. In addition, the indirect nature of the band gaps in these materials meant that they would be quite inefficient in optoelectronic devices.[40,41] To date, the p-type TCO with the highest reported conductivity is $CuCrO_2$/Mg, with a conductivity of 220 S cm^{-1},[29] two orders of magnitude smaller than that of the industry standard n-type TCO, In_2O_3/Sn ($\sim 10^4$ S cm^{-1}). The reason that $CuCrO_2$ has increased undoped and doped conductivity over the other delafossites is due to the involvement of Cr(III) in the formation of the VB. As Cr has a greater covalency with O than Al in $CuAlO_2$, for instance, the increased presence of Cr 3d states across the VB means that there is a greater delocalization of the hole states in $CuCrO_2$.[42] The role of the second cation can be as important to the effectiveness of the material as the Cu.[43]

The concept of the CMVB was then extended further to include other chalcogenide anions. Cu_2S and Cu_2Se display much higher levels of p-type conductivity than Cu_2O due to increased Cu−Ch mixing; however, their band gaps are much lower.[44−46] Hosono and coworkers identified that layered Cu-based oxychalcogenides could possess large band gaps and efficient Cu−Ch (Ch = S, Se) mixing at the VBM leading to more disperse bands and lower effective masses.[47] LaCuOS was first discovered to be a p-type TCO possessing a band gap of 3.1 eV. The conductivity when acceptor doped with Sr, however, was low at 2.6×10^{-1} S cm^{-1}.[47] LaCuOSe on the other hand displayed a larger conductivity, especially when doped with Mg producing a degenerate p-type material with a conductivity of 910 S cm^{-1}[48,49] arising from an increased hybridization of Cu 3d with Se 4p over S 3p,[48,50] however at the expense of transparency with a fundamental band gap of ∼2.8 eV[51]

Arising from the CMVB, the metastable compound Cu_3N with the anti-ReO_3 structure has been identified for solar absorber applications due to its ability to be bipolar and defect tolerant, i.e., the ability to maintain semiconducting properties when defects are present. The experimental band gap reported is 1.4 eV[52] which is ideal for photovoltaic applications.[53] Cu_3N has a calculated indirect band gap of 1.0 eV[54] (using DFT + U) and conductivities of $\sim 10^{-3}$ S cm^{-1}.[52] The defect tolerance of the material as identified by Zakutaev et al.[54] has been attributed to the nature of its band maxima and minima in that the top of the valence band is antibonding in character and contrariwise the bottom of the conduction band is bonding in its nature. This hybridization of the states at both the VBM and CBM is due to the N−Cu−N dumbbell motif in the structure, something that is seen in other compounds such as the delafossite $CuTaN_2$ which has a direct band gap of 1.5 eV and an indirect band gap of 1.4 eV.[55] The benefit of having these properties means that Cu_3N can accommodate both shallow p-type and n-type defects allowing for easy fabrication of compatible p−n junctions.

In this article, we extend the concept of CMVB further, by testing Cu−P mixing at the valence band maximum and examine the effects of Cu coordination on the valence band dispersion and therefore the effective masses. We have identified four compounds from the Inorganic Crystal Structure Database (ICSD), namely, MCuP (M = Mg, Ca, Sr, Ba), which possess group II cations that should not influence the makeup of the valence band maximum meaning that it should be dominated solely by Cu and P states. MgCuP, which was first reported by Mewis in 1979,[56] crystallizes in the *Pnma* crystal structure displaying tetrahedrally coordinated Cu with P, which itself is coordinated to four Cu atoms and five Mg atoms where Mg(II) displays square pyramidal coordination to P (shown in Figure 1a). CaCuP,[57] SrCuP,[57] and BaCuP[56] were also reported by Mewis in 1978−79, and all crystallize in the $P6_3/mmc$ structure as shown in Figure 1b,c. It is clear that there are planar layers of M(II) atoms (Ca, Sr, or Ba) repeated along the *c*-axis at a distance of $c/2$ each sitting between the two voids in the planar hexagonal networks of Cu−P coordinated to 6 Cu (3 above and 3 below) and 6 P (3 above and 3 below) as shown in Figure 1c. These hexagonal networks lie within the *ab* plane with the stacking along the *c*-axis which means that above every

DOI: 10.1021/acs.chemmater.6b03306
Chem. Mater. XXXX, XXX, XXX−XXX

Table 1. Calculated (PBE0) Lattice Parameters and Bond Lengths[a]

system	a/Å	b/Å	c/Å	Cu−P/Å	volume/Å^3
MgCuP	3.82 (3.84)	6.50 (6.53)	7.15 (7.17)	2.40 (2.46)	177.48 (179.61)
CaCuP	4.05 (4.06)	4.05 (4.06)	7.83 (7.80)	2.34 (2.34)	111.34 (111.12)
SrCuP	4.14 (4.15)	4.14 (4.15)	8.42 (8.48)	2.39 (2.39)	125.14 (126.18)
BaCuP	4.25 (4.24)	4.25 (4.24)	9.10 (9.01)	2.46 (2.45)	142.59 (140.15)

[a]Experimental values are shown in brackets.[56,57]

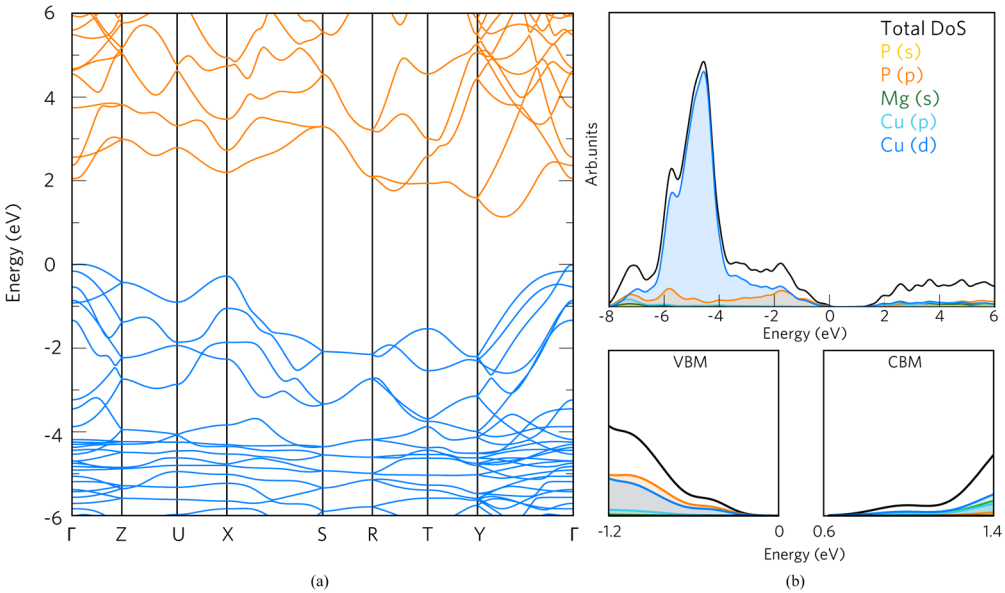

Figure 2. Calculated band structure diagram (a) and the density of states (DoS) (b) for MgCuP in the *Pnma* space group. For (a), the filled valence band is colored in blue and the unfilled conduction band is colored in orange. The valence band maximum (VBM) is centered at 0 eV in both cases. In (b), an expanded view of the VBM and the CBM is shown.

Cu atom there is a P atom and vice versa where each Cu forms a trigonal planar complex with three P anions (and likewise for P). To date, only crystallographic data on these materials exist with no analysis of their electronic properties.

Our hybrid density functional theory (hDFT) calculations, specifically using the PBE0 functional,[58,59] have demonstrated that the Cu−P mixing at the valence band maximum (VBM) does produce excellent dispersion comparable to that seen for excellent n-type materials. We critically discuss the importance of coordination environment in creating degenerate p-type materials and provide guidance for the design of novel p-type systems.

■ COMPUTATIONAL METHODOLOGY

The hybrid PBE0[58,59] functional using 25% exact Fock exchange was used for the electronic structure and total energy calculations as implemented in the VASP code.[60−63] Structural optimizations were carried out using a plane wave cut off energy of 400 eV and a k-point sampling of Γ-centered 7 × 7 × 4 for CaCuP, SrCuP, and BaCuP and Γ-centered 8 × 5 × 4 for MgCuP. The projector-augmented wave method (PAW)[64,65] was utilized to describe the interactions between the valence and the core electrons (Ca:[Ar], Sr:[Kr], Ba:[Xe], Mg:[Ne], Cu:[Ar], and P:[Ne]), and the structures were deemed to be converged when the forces on all the atoms were less than 0.01 eV Å^{-1}. The effective masses at the edges of the valence band and conduction band were calculated using the equation:

$$\frac{1}{m_{ij}^*} = \frac{\partial^2 E(k)}{\partial k_i \partial k_j}\frac{1}{\hbar^2} \quad (1)$$

where $E(k)$ is the energy of the band as a function of the wave vector k.

The calculated density of states (DoS) for CaCuP was weighted using the atomic orbital photoionization cross sections formulated by Yeh and Lindau[66] simulating valence band X-ray photoelectron spectroscopy (XPS) that can be compared directly with the experiment. A Gaussian broadening of 0.47 eV was also applied to match experimental broadening. This approach has been shown to give an accurate account of the electronic states that give rise to the XPS data.[67−70]

The optical absorption spectrum and optical transition matrix elements were calculated within the PAW method and transversal approximation.[71] This approach sums the absorption spectrum over all the direct valence band to conduction band transitions and ignores indirect and intraband absorptions.[72] This method has been applied to a number of previous works and is in good agreement with regards to the experiment, despite the electron−hole correlation not being addressed.[2,32,73−77]

■ EXPERIMENTAL METHODOLOGY

Ca (99.0%), Cu (99.9%), and P (99.9%) were obtained from SigmaAldrich. CaCuP was synthesized from the elements with an addition of 5% P over the required stoichiometry which was necessary due to evaporation. The starting materials were ground in an agate mortar and pestle in a nitrogen glovebox, sealed in a quartz tube under reduced pressure (c. 10^{-3} mbar), and heated at 500 °C, with heating and cooling rates of 5 °C/min for a total of 24 h with one intermittent regrinding which was carried out in the glovebox. Powder X-ray diffraction (XRD) was carried out on a STOE diffractometer in transmission geometry using Mo Kα radiation over the 2θ range of 2−40° with a step size of 0.05°. X-ray photoelectron spectroscopy (XPS) was carried out using a Thermo K-alpha spectrometer utilizing Al Kα

DOI: 10.1021/acs.chemmater.6b03306
Chem. Mater. XXXX, XXX, XXX−XXX

Table 2. Effective Masses (m^*) of Charge Carriers at the VBM and the CBM[a]

system	VBM/m_e	CBM/m_e
MgCuP	6.30 (Γ−Z) 0.15 (Γ−Y)	0.68 (CBM−Γ) 0.62 (CBM−Y)
CaCuP	0.25, *0.11* (Γ−M) 0.25, *0.11* (Γ−K) 0.79 (Γ−A)	0.39 (CBM−L) 0.90 (CBM−Γ)
SrCuP	0.27, *0.11* (Γ−M) 0.28, *0.11* (Γ−K) 0.87 (Γ−A)	3.50 (M−L) 0.30 (M−Γ)
BaCuP	0.28, *0.11* (Γ−M) 0.29, *0.11* (Γ−K) 0.81 (Γ−A)	0.39 (M−L) 0.22 (M−Γ)

[a]Italicized values refer to light hole effective masses.

Table 3. Approximate Percentages of States at the Valence Band Maximum (VBM) and the Conduction Band Minimum (CBM)

	VBM/%		CBM/%		
system	Cu	P	M(II)	Cu	P
MgCuP	4(p) + 42(d)	54(p)	22(s) + 5(p)	15(s) + 3(p) + 30(d)	19(s) + 6(p)
CaCuP	14(p) + 38(d)	48(p)	5(s) + 4(p) + 50(d)	34(p) + 2(d)	2(s) + 3(p)
SrCuP	14(p) + 38(d)	48(p)	5(s) + 2(p) + 51(d)	35(p) + 1(d)	6(p)
BaCuP	13(p) + 38(d)	49(p)	4(s) + 1(p) + 62(d)	24(p) + 3(d)	6(p)

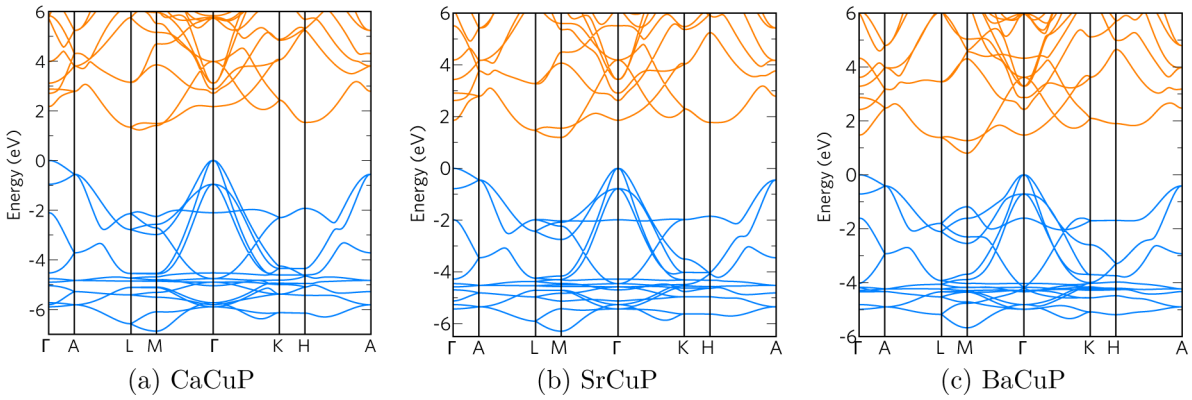

Figure 3. Calculated band structures of (a) CaCuP, (b) SrCuP, and (c) BaCuP in the $P6_3/mmc$ space group. The filled valence band is colored in blue, and the unfilled conduction band is colored in orange. The valence band maximum (VBM) is centered at 0 eV.

radiation and run in constant analyzer energy (CAE) mode. Survey and high resolution spectra were taken with a pass energy of 200 and 50 eV, respectively. For high resolution scans, a binding energy step size of 0.1 eV was used. The spectral resolution, measured as the full width at half-maximum (FWHM) of the Ag $3d_{5/2}$ peak on a clean Ag surface, was 0.9 eV under these conditions. In situ Ar ion etching was carried out using a 2000 eV Ar ion beam in a background Ar pressure of 2×10^{-7} mbar. The binding energy scale was corrected for charging by adjusting the adventitious C 1s peak to 284.6 eV. Optical measurements were taken using a PerkinElmer Fourier Transform Lambda 950 UV−vis spectrophotometer in diffuse reflectance geometry. Powder samples were packed into a holder presenting a surface area significantly larger than the incident beam and with sufficient thickness to ensure no transmission. Reflected light was measured using an integrating sphere, and reflectance values were converted using the Kubelka−Munk function to yield values proportional to absorption.[78] Conductivity measurements were carried out using an Ecopia HMS-3000 instrument and a van der Pauw electrode geometry.

■ RESULTS

The calculated structural parameters and Cu−P bond lengths for MgCuP, CaCuP, SrCuP, and BaCuP are presented in Table 1 and are in excellent agreement with the experimental values,[56,57] the slight underestimation of the data is due to DFT being carried out at the athermal limit in comparison to the room temperature conditions of the experimental analysis. Trends can be seen in the $P6_3/mmc$ structures as there is an increase in all lattice parameters and bond lengths down the group (Ca−Sr−Ba) which follows with the increase in ionic radii. The *a*/*b* and *c* lattice parameters stretch by around 5% and 14%, respectively, from CaCuP to BaCuP and the Cu−P bond lengths by ∼5%. The Cu−P bond lengths in MgCuP in the *Pnma* structure do not follow this trend and are in fact larger than those for CaCuP.

The PBE0 calculated band structure for MgCuP is displayed in Figure 2a. The VBM is situated at the high symmetry point Γ, and the conduction band minimum (CBM) is located between the points Y and Γ. MgCuP has an indirect band gap of 1.14 eV (the direct fundamental band gap at Γ is 2.06 eV). The top valence band from Γ−Y shows a decreased dispersion over the Γ−Z direction indicating a heavier hole effective mass, as shown in Table 2. The dispersion along Γ−Y leads to a hole effective mass of ∼0.15 m_e whereas Γ−Z possesses a much higher value of ∼6.30 m_e corresponding to a flatter band curvature seen clearly in Figure 2a. The CBM possesses relatively high dispersion in both the CBM−Γ and CBM−Y directions with electron effective masses of ∼0.68 and ∼0.62 m_e, respectively.

The calculated total and partial density of states (DoS) for MgCuP are presented in Figure 2b, and a collation of the percentages of states at the VBM and the CBM are shown in Table 3. The width of the upper valence band (VB) is approximately 8 eV with P 3s states seen from −8 to −7 eV mixed with Cu 3d + 3p, P 3p, and Mg 3s states. From −6 to −4 eV, the Cu 3d states dominate as shown with a large peak at −4.5 eV mixed with some P 3p states. Toward the VBM (0 eV), an increased hybridization of Cu 3d with P 3p states in a

DOI: 10.1021/acs.chemmater.6b03306
Chem. Mater. XXXX, XXX, XXX−XXX

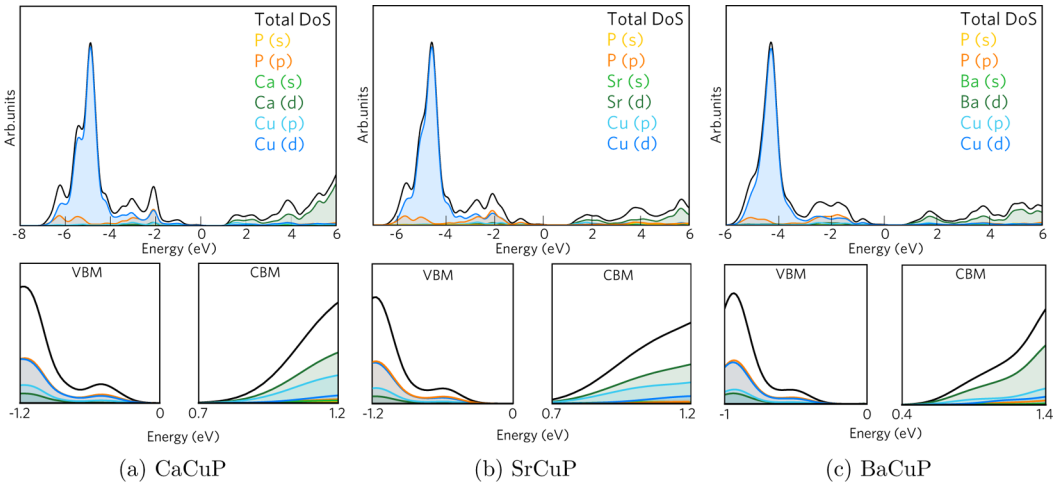

(a) CaCuP (b) SrCuP (c) BaCuP

Figure 4. Calculated density of states (DoS) for (a) CaCuP, (b) SrCuP, and (c) BaCuP. The valence band maximum (VBM) is set at 0 eV. Underneath each DoS is an expanded view of the VBM and CBM.

42:54 ratio is observed alongside some slight Cu 3p mixing (~4%). The CBM is predominantly of Cu d and s states mixed with a similar magnitude of Mg s states and P s + p states. From the CBM to 6 eV, a fairly uniform mixing of the P s + p, Cu p + d, and Mg s states is observed.

The band structures for CaCuP, SrCuP, and BaCuP are shown in Figure 3. The VBM is situated at Γ in all three compounds, and low hole effective masses are observed in the Γ−M and Γ−K directions. Two degenerate bands are present at the Γ point producing both extremely light and heavier effective masses. The lighter masses, being 0.11 m_e in all compounds, are insensitive to the group II cation whereas the heavier effective masses increase down the group (Ca−Sr−Ba) from ~0.25 m_e (CaCuP) to ~0.29 m_e (BaCuP). These values are competitive with and in some cases even surpass the industry standard n-type electron effective masses (~0.22, ~0.28, ~0.28, and ~0.22 m_e for In_2O_3,[79] ZnO,[80] SnO_2,[81] and $BaSnO_3$,[82] respectively) . From Γ−A however, the effective mass is limited to ~0.79−0.81 m_e and shows no particular trend down the group, yet these effective masses are superior to some of the top performing p-type TCOs such as $(Cu_2S_2)(Sr_3Sc_2O_5)$ and LaCuOSe/Mg (0.9 and 1.06 m_e, respectively).[49,76]

Similar to MgCuP, these materials also possess indirect band gaps, which decrease down group II; a maximum value of 1.23 eV is seen for CaCuP followed by 1.20 and 0.80 eV for SrCuP and BaCuP, respectively. The direct band gaps at Γ are 2.17, 1.86, and 1.48 eV, respectively. An increase in curvature at the CBM is seen from CaCuP to BaCuP resulting in an effective mass as low as ~0.22 m_e for BaCuP in the M−Γ direction. The CBM also shifts from between the L and M high symmetry points toward M down the group.

The DoS for the $P6_3/mmc$ structures are displayed in Figure 4. The valence band widths of CaCuP, SrCuP, and BaCuP are ~7, ~6.5, and ~6 eV, respectively. The electronic states are very similar in all three compounds; therefore, CaCuP is taken as an example for this analysis. From −7 to −4 eV, Cu 3d states dominate mixing with some P 3p states similar to that with MgCuP. The difference in intensity between these states decreases substantially from −4 to −2 eV where there is almost 50:50 overlap of the Cu d states with the P p states; however, there is an increase in Cu 3p mixing. From −2 to 0 eV (the VBM), the Cu 3p states tail off leaving the Cu 3d and P 3p states in a consistent 38:48 ratio from CaCuP to BaCuP with a remainder of ~14% Cu 3p states. The CBM consists of primarily unoccupied M(II) d states, the presence of which increase down the group (50−62%), alongside ~35% Cu p states and some negligible P p states. From 2 to 4 eV, a net increase in M(II) d states is seen together with hybridization from the Cu p states which decline leaving the region between 4 and 6 eV as primarily M(II) d states.

EXPERIMENTAL RESULTS

The powder XRD pattern from the sample of CaCuP was recorded, and the published structural model in the $P6_3/mmc$ space group[57] was used as a basis for Rietveld refinement using the EXPGUI and GSAS software and is shown in Figure 5.[83,84]

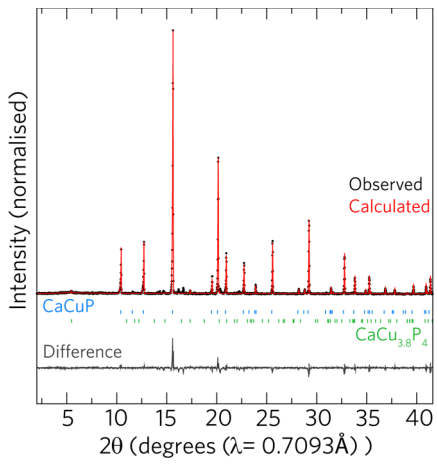

Figure 5. Powder X-ray diffraction pattern from CaCuP synthesized here (black) and calculated from the standard structure (red) with the difference between the calculated and observed intensities shown underneath in gray. The phase ticks for CaCuP and $CaCu_{3.8}P_4$ are shown in blue and green, respectively.

The initial fitting was carried out using the CaCuP phase alone, which led to a satisfactory fit of all intense peaks but some small peaks remained unaccounted for. A two phase refinement containing CaCuP and $CaCu_{3.8}P_2$ yielded an improvement in fit and accounted for several of the unknown peaks.[85] The CaCuP unit cell was refined in the $P6_3/mmc$ space group yielding lattice parameters of a = 4.070(1) Å and c = 7.826(2) Å which

DOI: 10.1021/acs.chemmater.6b03306
Chem. Mater. XXXX, XXX, XXX−XXX

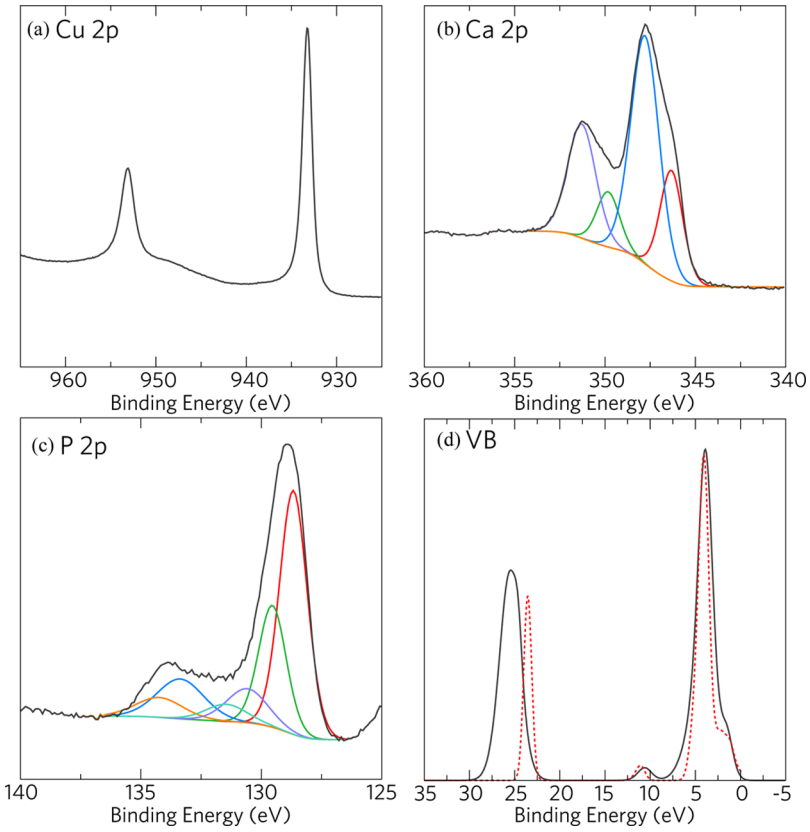

Figure 6. X-ray photoelectron spectra of CaCuP. (a) Cu 2p, (b) Ca 2p, and (c) P 2p regions are shown, with curve fitting as described in the text. The valence band region up to 35 eV binding energy is shown in (c) with the simulated VB XPS overlaid (red dashed line) taken from the PBE0 calculated DoS for CaCuP.

compare well with the reported structure.[57] The literature structure of $CaCu_{3.8}P_2$ was used without refinement of its unit cell. In the final refinement, an RWP value of 0.081 was obtained, and the impurity level of $CaCu_{3.8}P_2$ phase was 1.6(2) weight %.

Figure 6 displays the XPS spectra for the Cu 2p, Ca 2p, and P 2p regions alongside the valence band (VB) XPS. The surface of the as synthesized powder contained a significant amount of oxygen. Ar ion etching for 60 s using a 2000 eV Ar ion beam was able to reduce the level of oxygen suggesting that the oxidation was localized on the surface. High resolution spectra showed a symmetrical Cu $2p_{3/2}$ peak at 933.2 eV, corresponding to Cu(I). This assignment is supported by the lack of strong, sharp satellite peaks that typically accompany Cu(II) spectra.[86] Such satellite peaks arise from a $3d^9$ initial state that results on photemission in a series of screened and unscreened final states[87] and are detectable even with low concentrations of Cu(II) within a predominantly Cu(I) matrix.[88] The spectral region between the Cu 2p spin orbit doublet that we measure in CaCuP does show a very broad feature centered on 949.4 eV with fwhm of 8 eV. The origin of this feature is unknown, but it is unlike previously reported Cu(II) satellites, which are typically much sharper.[86−88] The feature may, therefore, be due to an as yet unassigned loss process. Given its position, some 16 eV above the Cu $2p_{3/2}$ peak, the feature may be due to valence band plasmon loss, which is typically seen in materials with similar valence band electron density at c. 20 eV to the high binding energy side of the main photoemission peak.[89] Unfortunately, the corresponding Cu $2p_{1/2}$ loss peak (if it were present) would be obscured by the O Auger line which overlaps on the binding energy scale at this photon energy. Further study is needed to ascertain the nature of the loss feature present in the Cu 2p spectrum.

Ca 2p spectra showed two overlapping doublets. The lower binding energy component has Ca $2p_{3/2}$ component at 346.3 eV (red trace, Figure 6b). We could find no reference of the XPS binding energy of Ca phosphide compounds. Ca_3P_2 itself is highly toxic and unstable, which may have precluded its measurement. However, CaS has been reported with a Ca $2p_{3/2}$ binding energy of 346.5 eV, very similar to our observed value.[90] Therefore, we assign the Ca $2p_{3/2}$ environment at 346.3 eV to Ca within the CaCuP structure. The other observed Ca 2p component, with Ca $2p_{3/2}$ binding energy of 347.8 eV (blue trace, Figure 6b) corresponds well to $Ca_3(PO_4)_2$ or $CaHPO_4$.[91] This indicates a level of oxidation of the surface as discussed above. No crystalline $Ca_3(PO_4)_2$ or $CaHPO_4$ was observed in XRD, again suggesting this is surface limited oxidation.

The P 2p region again was composed of overlapping peaks. Deconvolution showed that the principal chemical component (representing 66% of the P signal) was associated with a P $2p_{3/2}$ peak at 128.7 eV (red trace, Figure 6c), corresponding to phosphide compounds: for example, InP is reported with the same P $2p_{3/2}$ binding energy.[92] A higher binding energy component (representing 18% of the P signal) is also observed with a P $2p_{3/2}$ peak at 133.4 eV (blue trace, Figure 6c), corresponding to phosphate groups,[93] and consistent with the interpretation of the Ca 2p region given above. The remainder (c. 16% of the observed P signal) was fitted with a P $2p_{3/2}$ component at 130.5 eV (purple trace, Figure 6c) and may

DOI: 10.1021/acs.chemmater.6b03306
Chem. Mater. XXXX, XXX, XXX−XXX

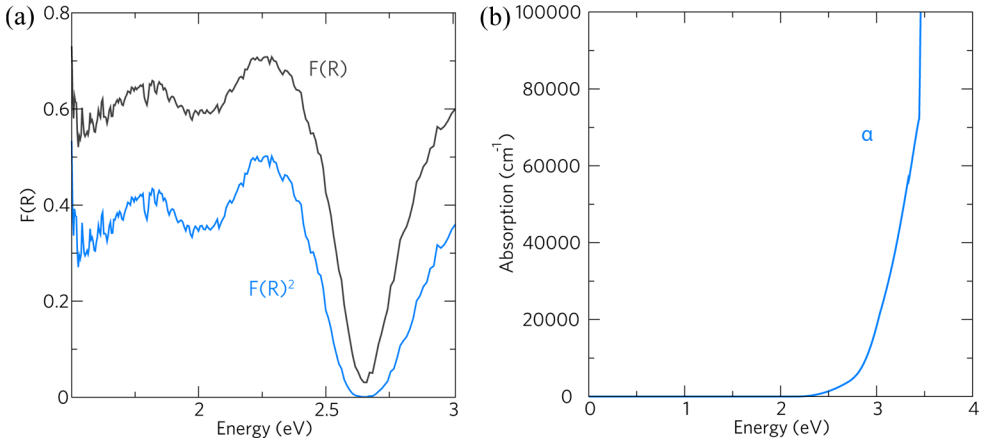

Figure 7. Diffuse reflectance optical spectra showing the Kubelka−Munk function F(R) and $F(R)^2$ is displayed in (a). The direct band gap calculated from the Poeppelmeier method is shown to be 2.78 eV. (b) Shows the calculated optical absorption spectrum using the PBE0 functional where a weak absorption onset at 2.17 eV and a strong absorption at 2.71 eV are seen.

originate from elemental P, which may be located at the sample surface due to evaporation during synthesis.

The valence band was recorded up to 30 eV binding energy. The main feature at low binding energy is a spectral maximum at 3.9 eV corresponding to Cu 3d electrons, which was confirmed by the excellent agreement with our simulated XPS (red dashed lines, Figure 6d). The onset of the valence band begins immediately at the Fermi level (BE = 0 eV), indicating a filled band immediately below the Fermi level, i.e., a p-type semiconductor or a metal. However, no Fermi edge was observed, meaning that if this is a metal the density of states at the Fermi level is low. This fits with our calculations of a very disperse valence band, with the Fermi level found near the VBM, most likely through Cu deficiency. The Ca 3p shallow core line appears at 25.5 eV.

Diffuse reflectance optical spectra were recorded in the interval of 1.5−3.5 eV. The Kubelka−Munk function, F(R), is taken to be proportional to absorption; this is valid if scattering is constant throughout the wavelength range used, which is a reasonable assumption.[78] There appears to be an absorption edge toward the higher energy range. Recently, Poeppelmeier and co-workers have proposed a method for accurate determination of the band gap in degenerately doped semiconductors.[94] This is similar to the well established Tauc method[95] but takes into account the presence of a large concentration of charge carriers. Using the Poeppelmeier method, plots of F(R) and $F(R)^2$ against energy were made and are displayed in Figure 7a alongside the simulated PBE0 optical absorption spectrum (b). The absorption edge of each plot was extrapolated to the x-axis ($y = 0$). For the F(R) plot, the extrapolated value E_1 = 2.66 eV. For the $F(R)^2$, the extrapolated value E_2 = 2.72 eV. According to the Poeppelmeier method, the band gap $E_g = 2E_2 - E_1$, which in this case gives 2.78 eV. Below the absorption edge, there are two strong absorption peaks located at 1.8 and 2.2 eV. The origin of these peaks is not clear. Cu(II) d−d transitions can occur in this energy range,[96] but XPS detects no Cu(II). While XPS detects calcium phosphate impurities at the surface, these are not expected to give rise to visible light absorption. The weight percentage of crystalline impurities (c. 1.7 wt %) is too low to effect strong absorption bands as seen here. The absorptions likely arise from as-yet unidentified defects within the CaCuP structure. Figure 7b displays the simulated PBE0 optical absorption in terms of the absorption coefficient α. A weak absorption onset is seen at ∼2.17 eV, and the stronger optical absorption occurs at ∼2.71 eV. These results are in excellent agreement with the experimental optical spectra in Figure 7a.

Conductivity measurements were carried out by forming a 12 mm diameter pellet, which was prepared by biaxial pressing at 1 tonne pressure followed by annealing at 300 °C for 4 h under nitrogen to sinter the particles. This yielded a pellet approximately 3 mm thick with a density of approximately 70%. The surface was polished to remove surface oxidation, and gold electrodes were sputtered in a van der Pauw geometry. Conductivity was then measured using a four point probe. A resistivity of $2.0 \times 10^{-3} \pm 0.2 \times 10^{-3}$ Ω cm was measured in this way. We were unable to record reliable Hall Effect data on the pellet.

■ DISCUSSION

Comparing the electronic structure of MgCuP to that of CaCuP, SrCuP, and BaCuP, it is clear that the electronic aspects differ due to the change in Cu coordination that occurs on going from the *Pnma* to $P6_3/mmc$ structure. Unlike CaCuP, SrCuP, and BaCuP, overall MgCuP displays only average hole effective masses at the VBM (despite the favorable Γ−Y mass of ∼0.15 m_e) and moderately heavy electron masses at the CBM. The excellent dispersion seen for CaCuP, SrCuP, and BaCuP in the Γ−M and the Γ−K directions can be attributed to excellent orbital overlap in the hexagonal layers. The Γ−A direction spans the c direction and therefore shows far less dispersion as the Cu and P atoms are coordinated only in the xy plane. MgCuP on the other hand should not be as prone to this anisotropic behavior as the tetrahedrally coordinated Cu is connected in a three-dimensional array throughout the lattice. This raises the question of whether, for copper phosphides, a trigonal planar Cu coordination is preferable over a tetrahedral coordination in terms of orbital overlap for dispersion in the valence band.

Cu coordination in all Cu^+-based systems is key to controlling the degree of overlap seen between the anion and cation states, which in turn controls the band dispersion at the VBM. For second row anions (O and N), Cu coordination is usually linear, as seen in Cu_2O[97,98] and delafossite $CuAlO_2$[40] structures as well as Cu_3N and $CuTaN_2$.[54,99] This unusually low coordination preference has originally been described by Orgel

DOI: 10.1021/acs.chemmater.6b03306
Chem. Mater. XXXX, XXX, XXX−XXX

in 1958 to be due to the closed shell metal cations such as Cu^+, Ag^+, and Hg^{2+} having a low energy difference between the first excited state d^9s^1 and the ground state d^{10} energy level.[100] This hybridized Cu [$3d_{z^2}$ + 4s] state is able to stabilize a low coordination level and is therefore the preferred configuration. In contrast, other d^{10} cations such as Zn^{2+} display a much higher separation between the d^9s^1 state and the d^{10} ground state meaning a higher coordination number is required for a lower energy configuration, as seen in, e.g., zinc blende or wurtzite ZnO where Zn is tetrahedrally coordinated to O.

Wurtzite-like β-$CuGaO_2$ was shown to yield a low band gap (~1.5 eV) and was considered quite promising for solar cell absorber applications.[101] A recent computational analysis, however, has shown that the tetrahedral coordination of the Cu^+ yields a very different valence band make up compared to that of the linear O−Cu−O coordination in the delafossite oxides.[102] For the delafossites, the Cu 3d and O 2p states overlap strongly, producing a relatively disperse VBM.[103−105] For β-$CuGaO_2$ and related systems, no mixing is observed at the VBM producing "flat" bands made soley of Cu 3d states.[102] Understanding the role of coordination in driving the valence band make up of a system is therefore vital.

Despite describing cuprous oxides and nitrides well, the Orgel's theory fails to give an understanding of why higher coordination numbers for Cu^+ are seen for chalcogenides such as the tetrahedrally coordinated $CuAlS_2$[99] and Cu_2S (which shows 3-fold coordination[106]). Instead, a push toward a more ionic model down the chalcogenides is necessary.[107] Tossel and Vaughan[106] provided another possibility taking into account the ligand interactions. In this model, the M d−L p (where M = Cu and L = anion such as O, S, Se, etc.) energy separation determines the coordination. The coordination should aim to reduce the spacing between the M d and the L p levels, in which, taking Cu_2O as an example where the spacing is large, a low coordination number would be favored.

An overview by Gaudin et al.[107] determined that the Cu 3d−O 2p interaction is in fact important in lowering the energy of the main Cu 4s−O 2p interaction thereby incorporating Orgel's theory. The authors also described another factor: the polarizing influence of the anion over the Cu^+ ion (Cu 3d electrons are poorly screened, making the ion quite polarizable), in which, for less polarizing anions (down the group and from right to left on the periodic table), this effect is lower and therefore the lower coordination number is less stable. It can then be said that higher coordination numbers are preferred for Se and Te copper compounds, as in KCuSe and KCuTe.[108] The presence of a third ion could also affect the polarization of the Cu cation by the anion, such as in the difference between Cu_2S and KCuS where coordination nos. of 3 and 2 are seen, respectively. A noticeable depletion in the electron density of the d electron cloud was observed for KCuS over Cu_2S indicating that the potassium cation contributes to the polarizability.[107]

The above explanations could help describe why for group II copper phosphides higher coordination numbers are preferred over copper oxides but also why a trigonal planar configuration is stabilized. Due to the polarizability argument described, P should adopt a higher coordination due to the low polarizability of P, as well as prefer a higher coordination down group II due to the decrease in polarizing power seen from Ca to Sr to Ba. However, from our calculations, CaCuP, SrCuP, and BaCuP all prefer the trigonal planar configuration, failing to adopt the same *Pnma* structure as MgCuP. Steric effects most likely play a role here as both phosphorus and the increasing M(II) cation down the group are relatively large. The tetrahedral coordination in these examples show a poorer orbital overlap than the trigonal planar configuration which can be seen in an increase in the Cu−P bond lengths. MgCuP in the $P6_3mmc$ space group (i.e., trigonal planar Cu−P) displays shorter Cu−P bond lengths over those in the *Pnma* structure (2.28 Å versus 2.40 Å) alongside lower overall effective masses.

What is seen in the $P6_3mmc$ structures is the increase in Cu−P bond length down the group and a detrimental effect on the hole effective masses and a concomitant lowering of the band gaps. An increase in the electron effective masses at the CBM is seen, however, as well as a decrease in the difference between the indirect and direct band gap. CaCuP, SrCuP, and BaCuP all possess a significant contribution from Cu 3p states at the VBM, from the p_x and p_y orbitals which add to the bonding, and hence the dispersion of the VBM. Taking into account the description by Tossel and Vaughan,[106] the P 3p and Cu 3d levels are closer in energy and hence a tetrahedral or trigonal planar is preferred over a linear configuration, as the Cu d−P p energy spacing is already minimal. Moving from a tetrahedral to a trigonal planar configuration also increases the crystal field splitting of Cu making the VBM more disperse pushing the antibonding states higher in energy and therefore reducing the ionization potential, which should favor hole formation.[109,110]

The experimental analysis on CaCuP supports our computational analysis and indicates that the material is a degenerate semiconductor with a relatively high p-type conductivity. What is most promising is that this high level of conductivity is for a nominally *undoped* pressed powder pellet and most likely originates from Cu deficiency. The nature of a pressed pellet means that this conductivity and mobility is limited by surface and interface effects. It is likely that this conductivity would be significantly boosted for a single crystal, making it competitive with the conductivities of the best n-type TCOs. The hole concentration could also be increased further with a suitable 1+ cation dopant for the divalent cation site.

The quest to find high performance p-type semiconductors for a range of applications is still ongoing.[8,111−115] Although CaCuP possesses a large optical band gap, this material is not transparent to visible light (E_g > 3.1 eV). However, the insights gained from this analysis of M(II)CuP and the interplay between structure and electronic properties provide design principles for the production of more effective p-type ability in semiconductor materials. As more and more technological breakthroughs occur for growth of materials, particularly designer layered compounds, increasingly complex systems can be fabricated.[116−118] To successfully create materials with trigonal Cu−P layers in this way could generate materials with tailored VBMs and band gaps, i.e., larger band gaps for transparent conducting applications.[119−121]

■ CONCLUSIONS

In order to gain insights into how to design excellent p-type transparent semiconductors, we have analyzed four ternary copper phosphide materials using hybrid density functional theory, finding low effective masses comparable to that of the highest performing n-type TCO. Synthesized powders of CaCuP have been created showing competitively high p-type conductivity in line with these results. We demonstrate that by extending the chemical modulation of the valence band method to include Cu−P interactions, a stronger hybridization with copper is observed which, together with a trigonal planar

DOI: 10.1021/acs.chemmater.6b03306
Chem. Mater. XXXX, XXX, XXX−XXX

coordination, produces highly favorable dispersion at the VBM. The design principles proposed herein can further the field of p-type semiconductors, opening up a pathway to the holy grail of degenerate p-type transparent conducting materials.

■ AUTHOR INFORMATION

Corresponding Author

*E-mail: d.scanlon@ucl.ac.uk.

Notes

The authors declare no competing financial interest.

■ ACKNOWLEDGMENTS

D.O.S. and R.G.P. acknowledge support from the SUPER-SOLAR Solar Energy Hub (EP/J017361/1) for the provision of a flexible funding call award and membership of the Materials Design Network. D.O.S. also acknowledges EPSRC (EP/N01572X/1). J.B. acknowledges EPSRC (EP/K016288/1). This work made use of the ARCHER UK National Supercomputing Service (http://www.archer.ac.uk), via our membership of the UK's HEC Materials Chemistry Consortium, which is funded by EPSRC (EP/L000202). The UCL Legion and Grace HPC Facilities (Legion@UCL and Grace@UCL) were also used in completion of this work. B.A.D.W. would like to acknowledge D.P. Howard and A.M. Ganose for useful discussions.

■ REFERENCES

(1) Odobel, F.; Le Pleux, L. L.; Pellegrin, Y.; Blart, E. New Photovoltaic Devices Based on the Sensitization of *p*-Type Semiconductors: Challenges and Opportunities. *Acc. Chem. Res.* **2010**, *43*, 1063−1071.

(2) Allen, J. P.; Scanlon, D. O.; Parker, S. C.; Watson, G. W. Tin Monoxide: Structural Prediction from First Principles Calculations with Van der Waals Corrections. *J. Phys. Chem. C* **2011**, *115*, 19916−19924.

(3) Kim, H.-J.; Lee, J.-H. Highly Sensitive and Selective Gas Sensors using *p*-Type Oxide Semiconductors: Overview. *Sens. Actuators, B* **2014**, *192*, 607−627.

(4) Fortunato, E.; Barquinha, P.; Martins, R. Oxide Semiconductor Thin-Film Transistors: A Review of Recent Advances. *Adv. Mater.* **2012**, *24*, 2945−2986.

(5) Gordon, R. G. Criteria for Choosing Transparent Conductors. *MRS Bull.* **2000**, *25*, 52−57.

(6) Beyer, W.; Hüpkes, J.; Stiebig, H. Transparent conducting oxide films for thin film silicon photovoltaics. *Thin Solid Films* **2007**, *516*, 147−154.

(7) Liu, H.; Avrutin, V.; Izyumskaya, N.; Özgür, U.; Morkoç, H. Transparent conducting oxides for electrode applications in light emitting and absorbing devices. *Superlattices Microstruct.* **2010**, *48*, 458−484.

(8) Hautier, G.; Miglio, A.; Ceder, G.; Rignanese, G.-M.; Gonze, X. Identification and Design Principles of Low Hole Effective Mass *p*-Type Transparent Conducting Oxides. *Nat. Commun.* **2013**, *4*, 2292.

(9) Scanlon, D. O.; Watson, G. W. On the Possibility of *p*-Type SnO_2. *J. Mater. Chem.* **2012**, *22*, 25236.

(10) Look, D. C. Electrical and Optical Properties of *p*-Type ZnO. *Semicond. Sci. Technol.* **2005**, *20*, S55−S61.

(11) Lany, S.; Zunger, A. Polaronic Hole Localization and Multiple Hole Binding of Acceptors in Oxide Wide-Gap Semiconductors. *Phys. Rev. B: Condens. Matter Mater. Phys.* **2009**, *80*, 1−5.

(12) Lany, S.; Zunger, A. Generalized Koopmans Density Functional Calculations Reveal the Deep Acceptor State of NO in ZnO. *Phys. Rev. B: Condens. Matter Mater. Phys.* **2010**, *81*, 1−5.

(13) Lyons, J. L.; Janotti, A.; Van De Walle, C. G. Why Nitrogen Cannot Lead to *p*-Type Conductivity in ZnO. *Appl. Phys. Lett.* **2009**, *95*, 252105.

(14) Catlow, C. R. a.; Sokol, A. a.; Walsh, A. Microscopic Origins of Electron and Hole Stability in ZnO. *Chem. Commun.* **2011**, *47*, 3386.

(15) Tran, Q.-P.; Fang, J.-S.; Chin, T.-S. Optical Properties and Boron Doping-Induced Conduction-Type Change in SnO_2 Thin Films. *J. Electron. Mater.* **2016**, *45*, 349−356.

(16) Pathak, T. K.; Kumar, V.; Swart, H.; Purohit, L. Effect of Doping Concentration on the Conductivity and Optical Properties of *p*-Type ZnO Thin Films. *Phys. B* **2016**, *480*, 31−35.

(17) Zhang, S. B.; Wei, S.-H. H.; Zunger, A. A Phenomenological Model for Systematization and Prediction of Doping Limits in II−VI and I−III−VI_2 Compounds. *J. Appl. Phys.* **1998**, *83*, 3192.

(18) Zhang, S. B.; Wei, S. H.; Zunger, A. Overcoming Doping Bottlenecks in Semiconductors and Wide-Gap Materials. *Phys. B* **1999**, *273*−*274*, 976−980.

(19) Zhang, S. B. The Microscopic Origin of the Doping Limits in Semiconductors and Wide-Gap Materials and Recent Developments in Overcoming These Limits: a Review. *J. Phys.: Condens. Matter* **2002**, *14*, R881−R903.

(20) Walsh, A.; Buckeridge, J.; Catlow, C. R. a.; Jackson, A. J.; Keal, T. W.; Miskufova, M.; Sherwood, P.; Shevlin, S. a.; Watkins, M. B.; Woodley, S. M.; Sokol, A. a. Limits to Doping of Wide Band Gap Semiconductors. *Chem. Mater.* **2013**, *25*, 2924−2926.

(21) Kawazoe, H.; Yasukawa, M.; Hyodo, H.; Kurita, M.; Yanagi, H.; Hosono, H. *P*-Type Electrical Conduction in Transparent Thin Films of $CuAlO_2$. *Nature* **1997**, *389*, 939−942.

(22) Scanlon, D. O.; Morgan, B. J.; Watson, G. W. Modeling the Polaronic Nature of *p*-Type Defects in Cu_2O: the Failure of GGA and GGA+U. *J. Chem. Phys.* **2009**, *131*, 124703.

(23) Scanlon, D. O.; Watson, G. W. Uncovering the Complex Behavior of Hydrogen in Cu_2O. *Phys. Rev. Lett.* **2011**, *106*, 1−4.

(24) Miao, M.-S.; Yarbro, S.; Barton, P. T.; Seshadri, R. Electron Affinities and Ionization Energies of Cu and Ag Delafossite Compounds: A Hybrid Functional Study. *Phys. Rev. B: Condens. Matter Mater. Phys.* **2014**, *89*, 045306.

(25) Scanlon, D. O.; Walsh, A.; Watson, G. W. Understanding the *p*-Type Conduction Properties of the Transparent Conducting Oxide $CuBO_2$: A Density Functional Theory Analysis. *Chem. Mater.* **2009**, *21*, 4568−4576.

(26) Snure, M.; Tiwari, A. $CuBO_2$: A *p*-Type Transparent Oxide. *Appl. Phys. Lett.* **2007**, *91*, 092123.

(27) Shi, L.-J.; Fang, Z.-J.; Li, J. First-Principles Study of *p*-Type Transparent Conductive Oxides $CuXO_2$ (X = Y, Sc, and Al). *J. Appl. Phys.* **2008**, *104*, 073527.

(28) Marquardt, M. a.; Ashmore, N. a.; Cann, D. P. Crystal Chemistry and Electrical Properties of the Delafossite Structure. *Thin Solid Films* **2006**, *496*, 146−156.

(29) Nagarajan, R.; Draeseke, a. D.; Sleight, a. W.; Tate, J. *p*-Type Conductivity in $CuCr_{1-x}Mg_xO_2$ Films and Powders. *J. Appl. Phys.* **2001**, *89*, 8022.

(30) Ueda, K.; Hase, T.; Yanagi, H.; Kawazoe, H.; Hosono, H.; Ohta, H.; Orita, M.; Hirano, M. Epitaxial Growth of Transparent *p*-Type Conducting $CuGaO_2$ Thin Films on Sapphire (001) Substrates by Pulsed Laser Deposition. *J. Appl. Phys.* **2001**, *89*, 1790.

(31) Kudo, A.; Yanagi, H.; Hosono, H.; Kawazoe, H. $SrCu_2O_2$: A *p*-Type Conductive Oxide with Wide Band Gap. *Appl. Phys. Lett.* **1998**, *73*, 220.

(32) Godinho, K. G.; Carey, J. J.; Morgan, B. J.; Scanlon, D. O.; Watson, G. W. Understanding Conductivity in $SrCu_2O_2$: Stability, Geometry and Electronic Structure of Intrinsic Defects from First Principles. *J. Mater. Chem.* **2010**, *20*, 1086−1096.

(33) Kandpal, H. C.; Seshadri, R. First-Principles Electronic Structure of the Delafossites ABO_2 (A = Cu, Ag, Au; B = Al, Ga, Sc, In, Y): Evolution of d^{10}-d^{10} Interactions. *Solid State Sci.* **2002**, *4*, 1045−1052.

(34) Kawazoe, H.; Yanagi, H.; Ueda, K.; Hosono, H. Transparent *p*-Type Conducting Oxides: Design and Fabrication of *p*-*n* Heterojunctions. *MRS Bull.* **2000**, *25*, 28−36.

(35) Benko, F.; Koffyberg, F. Opto-Electronic Properties of p and *n*-Type Delafossite, $CuFeO_2$. *J. Phys. Chem. Solids* **1987**, *48*, 431−434.

DOI: 10.1021/acs.chemmater.6b03306
Chem. Mater. XXXX, XXX, XXX−XXX

(36) Ingram, B.; Mason, T.; Asahi, R.; Park, K.; Freeman, A. Electronic Structure and Small Polaron Hole Transport of Copper Aluminate. *Phys. Rev. B: Condens. Matter Mater. Phys.* **2001**, *64*, 1−7.
(37) Ingram, B. J.; Harder, B. J.; Hrabe, N. W.; Mason, T. O.; Poeppelmeier, K. R. Transport and Defect Mechanisms in Cuprous Delafossites. 2. $CuScO_2$ and $CuYO_2$. *Chem. Mater.* **2004**, *16*, 5623−5629.
(38) Ingram, B. J.; Gonzàlez, G. B.; Mason, T. O.; Shahriari, D. Y.; Barnabè, A.; Ko, D.; Poeppelmeier, K. R. Transport and Defect Mechanisms in Cuprous Delafossites. 1. Comparison of Hydrothermal and Standard Solid-State Synthesis in $CuAlO_2$. *Chem. Mater.* **2004**, *16*, 5616−5622.
(39) Tate, J.; Ju, H. L.; Moon, J. C.; Zakutayev, A.; Richard, A. P.; Russell, J.; McIntyre, D. H. Origin of *p*-Type Conduction in Single-Crystal $CuAlO_2$. *Phys. Rev. B: Condens. Matter Mater. Phys.* **2009**, *80*, 165206.
(40) Scanlon, D. O.; Watson, G. W. Conductivity Limits in $CuAlO_2$ from Screened-Hybrid density functional theory. *J. Phys. Chem. Lett.* **2010**, *1*, 3195−3199.
(41) Brander, R. A Review of the Merits of Direct and Indirect Gap Semiconductors for Electroluminescence Devices. *Rev. Phys. Technol.* **1972**, *3*, 145−194.
(42) Scanlon, D. O.; Godinho, K. G.; Morgan, B. J.; Watson, G. W. Understanding Conductivity Anomalies in Cu-Based Delafossite Transparent Conducting Oxides: Theoretical Insights. *J. Chem. Phys.* **2010**, *132*, 024707.
(43) Scanlon, D. O.; Watson, G. W. Understanding the *p*-Type Defect Chemistry of $CuCrO_2$. *J. Mater. Chem.* **2011**, *21*, 3655.
(44) Nakano, Y.; Saeki, S.; Morikawa, T. Optical Bandgap Widening of *p*-Type Cu_2O Films by Nitrogen Doping. *Appl. Phys. Lett.* **2009**, *94*, 022111.
(45) Liu, G.; Schulmeyer, T.; BrÖtz, J.; Klein, A.; Jaegermann, W. Interface Properties and Band Alignment of Cu_2/CdS Thin Film Solar Cells. *Thin Solid Films* **2003**, *431−432*, 477−482.
(46) Riha, S. C.; Johnson, D. C.; Prieto, A. L. Cu_2Se Nanoparticles with Tunable Electronic Properties due to a Controlled Solid-State Phase Transition Driven by Copper Oxidation and Cationic Conduction. *J. Am. Chem. Soc.* **2011**, *133*, 1383−1390.
(47) Ueda, K.; Inoue, S.; Hirose, S.; Kawazoe, H.; Hosono, H. Transparent *p*-Type Semiconductor: LaCuOS Layered Oxysulfide. *Appl. Phys. Lett.* **2000**, *77*, 2701.
(48) Scanlon, D. O.; Buckeridge, J.; Catlow, C. R. A.; Watson, G. W. Understanding Doping Anomalies in Degenerate *p*-Type Semiconductor LaCuOSe. *J. Mater. Chem. C* **2014**, *2*, 3429.
(49) Hiramatsu, H.; Ueda, K.; Ohta, H.; Hirano, M.; Kikuchi, M.; Yanagi, H.; Kamiya, T.; Hosono, H. Heavy Hole Doping of Epitaxial Thin Films of a Wide Gap *p*-Type Semiconductor, LaCuOSe, and Analysis of the Effective Mass. *Appl. Phys. Lett.* **2007**, *91*, 012104.
(50) Liu, M. L.; Wu, L. B.; Huang, F. Q.; Chen, L. D.; Ibers, J. A. Syntheses, Crystal and Electronic Structure, and Some Optical and Transport Properties of LnCuOTe (Ln = La, Ce, Nd). *J. Solid State Chem.* **2007**, *180*, 62−69.
(51) Ueda, K.; Hosono, H.; Hamada, N. Energy Band Structure of LaCuOCh (Ch = S, Se and Te) Calculated by the Full-Potential Linearized Augmented Plane-Wave Method. *J. Phys.: Condens. Matter* **2004**, *16*, 5179−5186.
(52) Caskey, C. M.; Richards, R. M.; Ginley, D. S.; Zakutayev, A. Thin Film Synthesis and Properties of Copper Nitride, a Metastable Semiconductor. *Mater. Horiz.* **2014**, *1*, 424.
(53) Walsh, A.; Chen, S.; Wei, S.-H.; Gong, X.-G. Kesterite Thin-Film Solar Cells: Advances in Materials Modelling of Cu_2ZnSnS_4. *Adv. Energy Mater.* **2012**, *2*, 400−409.
(54) Zakutayev, A.; Caskey, C. M.; Fioretti, A. N.; Ginley, D. S.; Vidal, J.; Stevanovic, V.; Tea, E.; Lany, S. Defect Tolerant Semiconductors for Solar Energy Conversion. *J. Phys. Chem. Lett.* **2014**, *5*, 1117−1125.
(55) Yang, M.; Zakutayev, A.; Vidal, J.; Zhang, X.; Ginley, D. S.; DiSalvo, F. J. Strong Optical Absorption in $CuTaN_2$ Nitride Delafossite. *Energy Environ. Sci.* **2013**, *6*, 2994.
(56) Mewis, A. Darstellung und Struktur der Verbindungen MgCuP, BaCuP(As) und BaAgP(As). *Z. Naturforsch., B: J. Chem. Sci.* **1979**, *34*, 1373−1376.
(57) Mewis, A. ABX Verbindungen mit Ni_2 In-Struktur. Darstellung und Struktur der Verbindungen CaCuP(As), SrCuP(As), SrAgP(As) und EuCuAs. *Z. Naturforsch., B: J. Chem. Sci.* **1978**, *33*, 983−986.
(58) Adamo, C.; Barone, V. Toward Reliable Density Functional Methods Without Adjustable Parameters: The PBE0Model. *J. Chem. Phys.* **1999**, *110*, 6158.
(59) Paier, J.; Hirschl, R.; Marsman, M.; Kresse, G. The Perdew-Burke-Ernzerhof Exchange-Correlation Functional Applied to the G2−1 Test Set Using a Plane-Wave Basis Set. *J. Chem. Phys.* **2005**, *122*, 234102.
(60) Kresse, G.; Hafner, J. *Ab-initio* Molecular Dynamics for Liquid Metals. *Phys. Rev. B: Condens. Matter Mater. Phys.* **1993**, *47*, 558−561.
(61) Kresse, G.; Hafner, J. *Ab-initio* Molecular-Dynamics Simulation of the Liquid-Metal-Amorphous-Semiconductor Transition in Germanium. *Phys. Rev. B: Condens. Matter Mater. Phys.* **1994**, *49*, 14251−14269.
(62) Kresse, G.; Furthmüller, J. Efficiency of *Ab-Initio* Total Energy Calculations for Metals and Semiconductors Using a Plane-Wave Basis Set. *Comput. Mater. Sci.* **1996**, *6*, 15−50.
(63) Kresse, G.; Furthmüller, J. Efficient Iterative Schemes for *Ab-Initio* Total-Energy Calculations Using a Plane-Wave Basis Set. *Phys. Rev. B: Condens. Matter Mater. Phys.* **1996**, *54*, 11169−11186.
(64) Blöchl, P. E. Projector Augmented-Wave Method. *Phys. Rev. B: Condens. Matter Mater. Phys.* **1994**, *50*, 17953−17979.
(65) Kresse, G.; Joubert, D. From Ultrasoft Pseudopotentials to the Projector Augmented-Wave Method. *Phys. Rev. B: Condens. Matter Mater. Phys.* **1999**, *59*, 1758−1775.
(66) Yeh, J.; Lindau, I. Atomic Subshell Photoionization Cross Sections and Asymmetry Parameters: $1 \leqslant Z \leqslant 103$. *At. Data Nucl. Data Tables* **1985**, *32*, 1−155.
(67) Savory, C. N.; Ganose, A. M.; Travis, W.; Atri, R. S.; Palgrave, R. G.; Scanlon, D. O. An Assessment of Silver Copper Sulfides for Photovoltaic Applications: Theoretical and Experimental Insights. *J. Mater. Chem. A* **2016**, *4*, 12648.
(68) Bhachu, D. S.; Moniz, S. J. A.; Sathasivam, S.; Scanlon, D. O.; Walsh, A.; Bawaked, S. M.; Mokhtar, M.; Obaid, A. Y.; Parkin, I. P.; Tang, J.; Carmalt, C. J. Bismuth Oxyhalides: Synthesis, Structure and Photoelectrochemical Activity. *Chem. Sci.* **2016**, *7*, 4832−4841.
(69) Marchand, P.; Sathasivam, S.; Williamson, B. A. D.; Pugh, D.; Bawaked, S. M.; Basahel, S. N.; Obaid, A. Y.; Scanlon, D. O.; Parkin, I. P.; Carmalt, C. J. A Single-Source Precursor Approach to Solution Processed Indium Arsenide Thin Films. *J. Mater. Chem. C* **2016**, *4*, 6761−6768.
(70) Sathasivam, S.; Arnepalli, R. R.; Bhachu, D. S.; Lu, Y.; Buckeridge, J.; Scanlon, D. O.; Kumar, B.; Singh, K. K.; Visser, R. J.; Blackman, C. S.; Carmalt, C. J. Single Step Solution Processed GaAs Thin Films from $GaMe_3$ and $tBuAsH_2$ under Ambient Pressure. *J. Phys. Chem. C* **2016**, *120*, 7013−7019.
(71) Gajdoš, M.; Hummer, K.; Kresse, G.; Furthmüller, J.; Bechstedt, F. Linear Optical Properties in the Projector-Augmented Wave Methodology. *Phys. Rev. B: Condens. Matter Mater. Phys.* **2006**, *73*, 045112.
(72) Adolph, B.; Furthmüller, J.; Bechstedt, F. Optical Properties of Semiconductors Using Projector-Augmented Waves. *Phys. Rev. B: Condens. Matter Mater. Phys.* **2001**, *63*, 125108.
(73) Nie, X.; Wei, S.-H.; Zhang, S. B. Bipolar Doping and Band-Gap Anomalies in Delafossite Transparent Conductive Oxides. *Phys. Rev. Lett.* **2002**, *88*, 066405.
(74) Walsh, A.; Da Silva, J. L. F.; Yan, Y.; Al-Jassim, M. M.; Wei, S.-H. Origin of Electronic and Optical Trends in Ternary In_2O_3 $(ZnO)_n$ Transparent Conducting Oxides (n = 1.3,5): Hybrid Density Functional Theory Calculations. *Phys. Rev. B: Condens. Matter Mater. Phys.* **2009**, *79*, 073105.
(75) Walsh, A.; Yan, Y.; Huda, M. N.; Al-Jassim, M. M.; Wei, S.-H. Band Edge Electronic Structure of $BiVO_4$: Elucidating the Role of the Bi s and V d Orbitals. *Chem. Mater.* **2009**, *21*, 547−551.

DOI: 10.1021/acs.chemmater.6b03306
Chem. Mater. XXXX, XXX, XXX−XXX

(76) Scanlon, D. O.; Watson, G. W. (Cu_2S_2) ($Sr_3Sc_2O_5$)-A Layered, Direct Band Gap, *p*-Type Transparent Conducting Oxychalcogenide: A Theoretical Analysis. *Chem. Mater.* **2009**, *21*, 5435−5442.
(77) Allen, J. P.; Nilsson, M. K.; Scanlon, D. O.; Watson, G. W. Comparison of the Defective Pyrochlore and Ilmenite Polymorphs of $AgSbO_3$ using GGA and hybrid DFT. *Phys. Rev. B: Condens. Matter Mater. Phys.* **2011**, *83*, 035207.
(78) Kubelka, P. New Contributions to the Optics of Intensely Light-Scattering Materials Part I. *J. Opt. Soc. Am.* **1948**, *38*, 448.
(79) Preissler, N.; Bierwagen, O.; Ramu, A. T.; Speck, J. S. Electrical Transport, Electrothermal Transport, and Effective Electron Mass in Single-Crystalline In_2O_3 films. *Phys. Rev. B: Condens. Matter Mater. Phys.* **2013**, *88*, 085305.
(80) Button, K. J.; Cohn, D. R.; Von Ortenbert, M.; Lax, B.; Mollwo, E.; Helbig, R. Zeeman Splitting of Anomalous Shallow Bound States in ZnO. *Phys. Rev. Lett.* **1972**, *28*, 1637−1639.
(81) Button, K. J.; Fonstad, C. G.; Dreybrodt, W. *Determination of the Electron Masses in Stannic Oxide by Submillimeter Cyclotron Resonance* **1971**, *4*, 4539−4541.
(82) Scanlon, D. O. Defect Engineering of $BaSnO_3$ for High-Performance Transparent Conducting Oxide Applications. *Phys. Rev. B: Condens. Matter Mater. Phys.* **2013**, *87*, 161201.
(83) Toby, B. H. EXPGUI, a Graphical User Interface for GSAS. *J. Appl. Crystallogr.* **2001**, *34*, 210−213.
(84) Larson, A.; Dreele, R. V. *General Structure Analysis System (GSAS)*; Los Alamos National Laboratory Report LAUR 86-748; Los Alamos National Laboratory: Los Alamos, NM, 2004.
(85) Mewis, A. Darstellung und Struktur der Verbindung $CaCu_4P_2$. *Z. Naturforsch., B: J. Chem. Sci.* **1980**, *35*, 942−945.
(86) Ghijsen, J.; Tjeng, L. H.; van Elp, J.; Eskes, H.; Westerink, J.; Sawatzky, G. A.; Czyzyk, M. T. Electronic Structure of Cu_2O and CuO. *Phys. Rev. B: Condens. Matter Mater. Phys.* **1988**, *38*, 11322−11330.
(87) Shin, D.; Foord, J. S.; Egdell, R. G.; Walsh, A. Electronic Structure of $CuCrO_2$ Thin Films Grown on Al_2O_3(001) by Oxygen Plasma Assisted Molecular Beam Epitaxy. *J. Appl. Phys.* **2012**, *112*, 113718.
(88) Deuermeier, J.; Gassmann, J.; Brötz, J.; Klein, A. Reactive Magnetron Sputtering of Cu_2O: Dependence on Oxygen Pressure and Interface Formation with Indium Tin Oxide. *J. Appl. Phys.* **2011**, *109*, 113704.
(89) Egdell, R. G.; Henrich, V. E.; Bowdler, R.; Sekine, T. On the Difference in Valence Electron Plasmon Energy and Density of States Between Beta- and Cubic-Si_3N_4. *J. Appl. Phys.* **2003**, *94*, 6611.
(90) Franzen, H.; Merrick, J.; Umaña, M.; Khan, A.; Peterson, D.; McCreary, J.; Thorn, R. XPS Spectra and Crystalline Potentials in Alkaline-Earth Chalcogenides and Hydrides. *J. Electron Spectrosc. Relat. Phenom.* **1977**, *11*, 439−443.
(91) Demri, B.; Muster, D. XPS Study of Some Calcium Compounds. *J. Mater. Process. Technol.* **1995**, *55*, 311−314.
(92) Clark, D.; Fok, T.; Roberts, G.; Sykes, R. An Investigation by Electron Spectroscopy for Chemical Analysis of Chemical Treatments of the (100) Surface of *n*-type InP Epitaxial Layers for Langmuir Film Deposition. *Thin Solid Films* **1980**, *70*, 261−283.
(93) Streubel, P.; Franke, R.; Chassé, T.; Fellenberg, R.; Szargan, R. Chemical State Information from Photoelectron and Auger Electron Lines - Investigation of Potential and Relaxation Effects of Solid Silicon and Phosphorus Compounds. *J. Electron Spectrosc. Relat. Phenom.* **1991**, *57*, 1−13.
(94) Dolgonos, A.; Mason, T. O.; Poeppelmeier, K. R. Direct Optical Band Gap Measurement in Polycrystalline Semiconductors: A Critical Look at the Tauc Method. *J. Solid State Chem.* **2016**, *240*, 43−48.
(95) Tauc, J.; Grigorovici, R.; Vancu, A. Optical Properties and Electronic Structure of Amorphous Germanium. *Phys. Status Solidi B* **1966**, *15*, 627−637.
(96) Jianmin, L.; Yugeng, Z. The d-d Transition Spectra of Copper (II) Complexes in Different Coordination Environment. Study on $Cu(TTA)_2$ and $Cu_2(sacch)_4(Im)_4$. *Cryst. Res. Technol.* **1991**, *26*, 331−337.
(97) Zuo, J. M.; Kim, M.; O'Keeffe, M.; Spence, J. C. H. Direct Observation of d-Orbital Holes and Cu-Cu Bonding in Cu_2O. *Nature* **1999**, *401*, 49−52.
(98) Scanlon, D. O.; Watson, G. W. Undoped n-Type Cu_2O: Fact or Fiction? *J. Phys. Chem. Lett.* **2010**, *1*, 2582−2585.
(99) Hahn, U.; Weber, W. Electronic Structure and Chemical-Bonding Mechanism of Cu_3N, Cui_3NPd, and Related Cu(I) Compounds. *Phys. Rev. B: Condens. Matter Mater. Phys.* **1996**, *53*, 12684.
(100) Orgel, L. Stereochemistry of Metals of the B Sub-Groups. Part I. Ions with Filled & Electron Shells. *J. Chem. Soc.* **1958**, 4186−4190.
(101) Omata, T.; Nagatani, H.; Suzuki, I.; Kita, M.; Yanagi, H.; Ohashi, N. Wurtzite $CuGaO_2$: A New Direct and Narrow Band Gap Oxide Semiconductor Applicable as a Solar Cell Absorber. *J. Am. Chem. Soc.* **2014**, *136*, 3378−3381.
(102) Scanlon, D. O.; Walsh, A. Polymorph Engineering of $CuMO_2$ (M = Al, Ga, Sc, Y) Semiconductors for Solar Energy Applications: From Delafossite to Wurtzite. *Acta Crystallogr., Sect. B: Struct. Sci., Cryst. Eng. Mater.* **2015**, *71*, 702−706.
(103) Arnold, T. X-ray Spectroscopic Study of the Electronic Structure of CuCrO 2. *Phys. Rev. B: Condens. Matter Mater. Phys.* **2009**, *79*, 075102.
(104) Shin, D. Comparative Study of Bandwidths in Copper Delafossites from X-ray Emission Spectroscopy. *Phys. Rev. B: Condens. Matter Mater. Phys.* **2009**, *80*, 233105.
(105) Scanlon, D. O.; Walsh, A.; Morgan, B. J.; Watson, G. W.; Payne, D. J.; Egdell, R. G. Effect of Cr Substitution on the Electronic Structure of $CuAl_{1-x}Cr_xO_2$. *Phys. Rev. B: Condens. Matter Mater. Phys.* **2009**, *79*, 035101.
(106) Tossell, J. A.; Vaughan, D. J. Relationships Between Valence Orbital Binding Energies and Crystal Structures in Compounds of Copper, Silver, Gold, Zinc, Cadmium, and Mercury. *Inorg. Chem.* **1981**, *20*, 3333−3340.
(107) Gaudin, E.; et al. Some Factors Governing Ag+ and Cu+ Low Coordination in Chalcogenide Environments. *J. Solid State Chem.* **2001**, *160*, 212−221.
(108) Savelsberg, G.; Schäfer, H. Ternäre Pnictide und Chalkogenide von Alkalimetallen und IB-bzw. *Z. Naturforsch., B: J. Chem. Sci.* **1978**, *33*, 370−373.
(109) Buckeridge, J.; Butler, K. T.; Catlow, C. R. A.; Logsdail, A. J.; Scanlon, D. O.; Shevlin, S. A.; Woodley, S. M.; Sokol, A. A.; Walsh, A. Polymorph Engineering of TiO_2: Demonstrating how Absolute Reference Potentials are Determined by Local Coordination. *Chem. Mater.* **2015**, *27*, 3844−3851.
(110) Burbano, M.; Scanlon, D. O.; Watson, G. W. Sources of Conductivity and Doping Limits in CdO from Hybrid Density Functional Theory. *J. Am. Chem. Soc.* **2011**, *133*, 15065−15072.
(111) Bhatia, A.; Hautier, G.; Nilgianskul, T.; Miglio, A.; Sun, J.; Kim, H. J.; Kim, K. H.; Chen, S.; Rignanese, G.-M.; Gonze, X.; Suntivich, J. High-Mobility Bismuth-Based Transparent *p*-Type Oxide from High-Throughput Material Screening. *Chem. Mater.* **2016**, *28*, 30−34.
(112) Aksit, M.; Kolli, S. K.; Slauch, I. M.; Robinson, R. D. Misfit Layered $Ca_3Co_4O_9$ as a High Figure of Merit *p*-Type Transparent Conducting Oxide Film Through Solution Processing. *Appl. Phys. Lett.* **2014**, *104*, 161901.
(113) Arca, E.; Fleischer, K.; Shvets, I. V. Magnesium, Nitrogen Codoped Cr_2O_3: A *p*-Type Transparent Conducting Oxide. *Appl. Phys. Lett.* **2011**, *99*, 111910.
(114) Wei, R.; Tang, X.; Hu, L.; Hui, Z.; Yang, J.; Luo, H.; Luo, X.; Dai, J.; Song, W.; Yang, Z.; Zhu, X.; Sun, Y. Transparent Conducting *p*-Type Thin Films of c-Axis Self-Oriented $Bi_2Sr_2Co_2O_y$ with High Figure of Merit. *Chem. Commun.* **2014**, *50*, 9697.
(115) Zhang, K. H. L.; Du, Y.; Papadogianni, A.; Bierwagen, O.; Sallis, S.; Piper, L. F. J.; Bowden, M. E.; Shutthanandan, V.; Sushko, P. V.; Chambers, S. A. Perovskite Sr-Doped $LaCrO_3$ a New *p*-Type Transparent Conducting Oxide. *Adv. Mater.* **2015**, *27*, 5191−5195.
(116) Palgrave, R. G.; Borisov, P.; Dyer, M. S.; McMitchell, S. R. C.; Darling, G. R.; Claridge, J. B.; Batuk, M.; Tan, H.; Tian, H.; Verbeeck, J.; Hadermann, J.; Rosseinsky, M. J. Artificial Construction of the

DOI: 10.1021/acs.chemmater.6b03306
Chem. Mater. XXXX, XXX, XXX−XXX

Layered Ruddlesden–Popper Manganite $La_2Sr_2Mn_3O_{10}$ Reflection High Energy Electron Diffraction Monitored Pulsed Laser Deposition. *J. Am. Chem. Soc.* **2012**, *134*, 7700–7714.

(117) Haeni, J. H.; Theis, C. D.; Schlom, D. G.; Tian, W.; Pan, X. Q.; Chang, H.; Takeuchi, I.; Xiang, X.-D. Epitaxial Growth of the First Five Members of the $Sr_{n+1}Ti_nO_{3n+1}$ Ruddlesden-Popper Homologous Series. *Appl. Phys. Lett.* **2001**, *78*, 3292.

(118) Tian, W.; Pan, X. Q.; Haeni, J. H.; Schlom, D. G. Transmission Electron Microscopy Study of n = 1–5 $Sr_{n+1}Ti_nO_{3n+1}$ Epitaxial Thin Films. *J. Mater. Res.* **2001**, *16*, 2013–2026.

(119) Johnson, R. W.; Hultqvist, A.; Bent, S. F. A Brief Review of Atomic Layer Deposition: from Fundamentals to Applications. *Mater. Today* **2014**, *17*, 236–246.

(120) Hiramatsu, H.; Ueda, K.; Ohta, H.; Orita, M.; Hirano, M.; Hosono, H. Heteroepitaxial Growth of a Wide-Gap *p*-Type Semiconductor, LaCuOS. *Appl. Phys. Lett.* **2002**, *81*, 598.

(121) Su, G.; Hadjiev, V. G.; Loya, P. E.; Zhang, J.; Lei, S.; Maharjan, S.; Dong, P.; Ajayan, P. M.; Lou, J.; Peng, H. Chemical Vapor Deposition of Thin Crystals of Layered Semiconductor SnS_2 for Fast Photodetection Application. *Nano Lett.* **2015**, *15*, 506–513.

DOI: 10.1021/acs.chemmater.6b03306
Chem. Mater. XXXX, XXX, XXX–XXX